
Visual Sparse Steering: Improving Zero-shot Image Classification with Sparsity Guided Steering Vectors

Gerasimos Chatzoudis^{1*} Zhuowei Li¹ Gemma E. Moran² Hao Wang¹ Dimitris N. Metaxas¹

¹Department of Computer Science, Rutgers University

²Department of Statistics, Rutgers University

Abstract

Steering vision foundation models at inference time without retraining or access to large labeled datasets is a desirable yet challenging objective, particularly in dynamic or resource-constrained settings. In this paper, we introduce Visual Sparse Steering (VS2), a lightweight, test-time method that guides vision models using steering vectors derived from sparse features learned by top- k Sparse Autoencoders without requiring contrastive data. Specifically, VS2 surpasses zero-shot CLIP by 4.12% on CIFAR-100, 1.08% on CUB-200, and 1.84% on Tiny-ImageNet. We further propose VS2⁺⁺, a retrieval-augmented variant that selectively amplifies relevant sparse features using pseudo-labeled neighbors at inference time. With oracle positive/negative sets, VS2⁺⁺ achieves absolute top-1 gains over CLIP zero-shot of up to 21.44% on CIFAR-100, 7.08% on CUB-200, and 20.47% on Tiny-ImageNet. Interestingly, VS2 and VS2⁺⁺ raise per-class accuracy by up to 25% and 38%, respectively, showing that sparse steering benefits specific classes by disambiguating visually or taxonomically proximate categories rather than providing a uniform boost. Finally, to better align the sparse features learned through the SAE reconstruction task with those relevant for downstream performance, we propose Prototype-Aligned Sparse Steering (PASS). By incorporating a prototype-alignment loss during SAE training, using labels only during training while remaining fully test-time unsupervised, PASS consistently, though modestly, outperforms VS2, achieving a 6.12% gain over VS2 only on CIFAR-100 with ViT-B/32.

1 Introduction

Foundation Models (FMs) have exhibited strong generalization capabilities across a wide range of domains, from classification tasks to open-ended generation [1, 2, 3, 4, 5]. Despite their impressive performance, these models largely function as black boxes, restricting their controllability, and reliability in practice. The standard approach to edit a model’s behavior involves first collecting a labeled dataset resembling the target objective, followed by a supervised fine-tuning (SFT) procedure upon the holistic [6, 7] or partial (*e.g.*, PEFT [8, 9, 10]) parameter space. Nevertheless, this procedure is cumbersome and can become prohibitively expensive given the model scale. Consequently, Steering Vector (SV) methods [11, 12, 13], as an alternative, have gained popularity in the Large Language Model (LLM) domain as they can effectively modulate the model’s generation at inference-time in a training-free manner. While SVs have shown promise in LLMs, their functionality in the vision domain remains unclear.

In this work, we investigate the functionality of steering vectors in vision foundation models (VFM). In particular, we use zero-shot classification tasks as a testbed to explore how SVs can be leveraged to

*Correspondence to: Gerasimos Chatzoudis <gerasimos.chatzoudis@rutgers.edu> and Zhuowei Li <z1502@cs.rutgers.edu>.

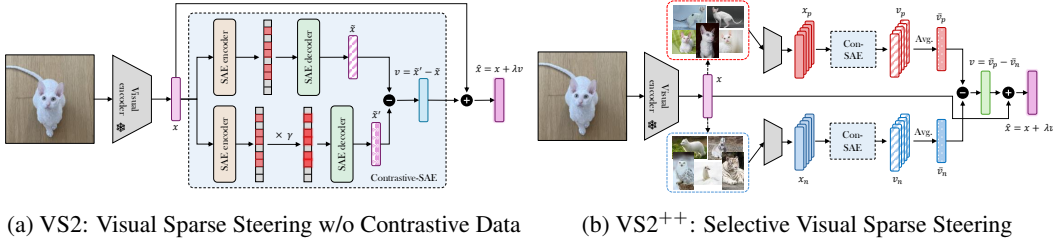


Figure 1: Overview of VS2 and VS2⁺⁺. At inference, VS2 finds sparse latent concepts, and steers the original embedding towards the direction of amplifying those sparse features. When additional caching data is available, VS2 selectively enhances certain features while suppressing others in a contrastive manner.

upweight relevant visual features. Conventional SVs operate by first constructing a directional vector within the latent space to indicate a desired change of the functionality. It then linearly combines the directional vector with the original latent embeddings to craft output embeddings. In LLMs, SVs rely on two symbolic anchors that are inherently interpretable to determine the functional direction of the SV. For example, a *happiness* SV can be extracted using the latent embedding arithmetic corresponding to Happy - Sad. The formulation of SVs in LLM poses two critical challenges in vision domain. Given an image at inference-time: (1) Unlike symbolic language tokens, there exists tremendous redundancy in visual representations; consequently, it is unclear *what features should be steered*; (2) Without inherently interpretable anchors (e.g., happy, sad), *towards which direction to steer* is not obvious.

To address the aforementioned challenges, we propose **Visual Sparse Steering (VS2)**. Drawing inspiration from the interpretability provided by sparse auto-encoders (SAEs) [14, 15, 16, 17], we hypothesize that the sparse features in a SAE’s latent space can capture key aspects of a visual embedding. VS2 upweights these features equally to construct a steering vector for classification. This equal upweighting of features is imprecise in that we expect different features to be more relevant than others for classification tasks. Despite this, we show that the simple equal upweighting of features still improves zero-shot classification.

To construct a more precise steering vector, we propose VS2⁺⁺, which leverages additional unlabeled data to construct steering vectors for classification. For a given target image, VS2⁺⁺ retrieves the Top-N most similar visual embeddings, and constructs positive and negative groups according to generated pseudo labels². The VS2⁺⁺ SV is then constructed via subtracting the average SAE features of the negative group from the positive group. Intuitively, VS2⁺⁺ upweights the SAE features most relevant for distinguishing the positive and negative groups. In summary, VS2 and VS2⁺⁺ aim to enhance downstream classification performance while retaining the interpretability of SAEs. To further align the sparse features learned through the SAE reconstruction task with those important for downstream performance, we propose Prototype-Aligned Sparse Steering (PASS).

VS2 consistently outperforms all baseline methods across all datasets and ViT backbones, surpassing zero-shot CLIP [18] by 3.45% and 4.12% on CIFAR-100, 0.93% and 1.08% on CUB-200, and 1.50% and 1.84% on Tiny-ImageNet with ViT-B/32 and ViT-B/16 backbones, respectively, without any external data or supervision. When using external unlabeled image data, VS2⁺⁺ achieves absolute top-1 gains over CLIP zero-shot of up to 21.44% on CIFAR-100, 7.08% on CUB-200, and 20.47% on Tiny-ImageNet. Finally, by adding a lightweight prototype-alignment loss during SAE training (labels used only in training, still test-time unsupervised) PASS consistently, though slightly, outperforms VS2, offering a marginal 6.12% gain over VS2 only on CIFAR-100 with ViT-B/32. Our main contributions are:

- We investigate the functionality of steering vectors in vision domain, and propose VS2 that leverages sparse feature learning to construct steering vectors for zero-shot classification.

²In practice, pseudo labels can be gathered using either unsupervised clustering methods or zero-shot classification results

- We further propose VS2⁺⁺ for scenarios where additional unlabeled data is available to selectively amplify important concepts. In this case, we use VS2 on pseudo-positive and -negative data to upweight relevant features for classification.
- We propose Prototype-Aligned Sparse Steering (PASS), a lightweight method that introduces a prototype-alignment loss during SAE training using class labels only during training while remaining fully test-time unsupervised.
- We empirically demonstrate that VS2, VS2⁺⁺, and PASS can leverage SAEs to substantially improve zero-shot classification performance, outperforming baseline methods by a large margin under their corresponding regimes, while also retaining interpretability.

2 Related Work

Mechanistic Interpretability and Sparse Autoencoders. Several traditional approaches exist for interpretability in vision models, including feature visualization [19, 20, 21] and network dissection [22, 23]. Mechanistic interpretability seeks to systematically analyze and understand neural networks [24, 25], but it faces challenges due to polysemantic neurons i.e. units that activate in response to multiple, seemingly unrelated inputs [26]. This phenomenon arises from superposition, where networks encode more features than the available dimensions allow, forcing different concepts to share the same activations [26]. Sparse Autoencoders (SAEs) have been shown to mitigate superposition by applying sparse dictionary learning to model internals [27, 28]. Recent efforts have leveraged SAEs to uncover interpretable features within LLMs, revealing latent units tied to grammar rules, style patterns, and factual knowledge [29, 30, 31]. [32] refines this by training autoencoders on embedding differences to disentangle multiple concept shifts, enabling precise interventions in model activations without requiring direct supervision. While these methods focus on language models, our work extends sparse steering to the vision domain, where applications of SAEs to **vision models** remain *comparatively* underexplored.

While some studies investigate SAEs for exploratory feature analysis or generative modeling in the visual domain [14, 15, 16, 17], they primarily address concept discovery rather than performance enhancement. Other attempts in the vision domain try to create new SAE architectures for concept extraction [33, 34]. In contrast, our method leverages SAEs not only to interpret but also to *actively steer* vision models, yielding classification improvements alongside interpretable latent representations.

Similar to our line of work, [35] validate CLIP’s steerability and its efficacy in suppressing typographic attacks. Patch-SAE [36] improves zero-shot classification by applying latent masking based on class-level activations. Specifically, it aggregates SAE activations from the training split to identify the top- k most frequently activated latents per class, which are then used to mask active latents at test time. Our approach differs in a key aspect: **we do not rely on activation aggregations from the same class in training** but our method is instead fully test-time unsupervised. This design avoids reliance on class-conditioned statistics, making our approach more flexible and applicable to a wide range of tasks without requiring dataset-specific activation distributions. Specifically, our method (i) operates entirely in the vision latent space, (ii) requires no class labels, external vocabularies, or gradient updates, and (iii) improves zero-shot classification by amplifying sparse SAE features rather than replacing or suppressing activations.

Steering Vectors. Steering vector (SV) methods [11, 37, 38, 39], also known as representation engineering [12], construct a directional vector (or task vector) and apply it in the latent space to change the target model’s behavior at inference-time. SVs have gained popularity in LLM/MLLM domain as it can improve generation security [13], promoting truthfulness [40], mitigating hallucination [41], as well as improving inference efficiency [13, 42]. Interestingly, prior work has shown that in VLMs, *visual cues are influenced by language*, and that *biases in the model’s response can be steered through simple natural language prompts* [43]. In contrast, we differentiate from this line of work by focusing on Vision Foundation Models directly steering representations in the latent space *without any external language signal*.

Recent work has demonstrated that sparse representations can improve interpretability and disentanglement in steering directions [44, 45]. Unlike these methods, which rely on supervised contrastive examples or training data, our approach discovers meaningful sparse directions in vision models

without requiring labeled concept pairs, making it more adaptable to general visual representations. Furthermore, its applicability to vision foundation models (VFM) remains unclear. The proposed visual sparse steering (VS2) method demonstrates that SV methods, combined with sparse autoencoders, can be utilized to enhance image features, improving zero-shot classification.

3 Method

3.1 Preliminaries

Sparse Autoencoder (SAE). A SAE consists of an encoder-decoder pair that maps an input vector \mathbf{x} into a latent representation \mathbf{z} , then reconstructs \mathbf{x} from \mathbf{z} . Formally, we define the encoder as:

$$\mathbf{z} = \text{ReLU}\left(\mathbf{W}_{\text{enc}}(\mathbf{x} - \mathbf{b}_{\text{pre}}) + \mathbf{b}_{\text{enc}}\right), \quad (1)$$

where $\mathbf{W}_{\text{enc}} \in \mathbb{R}^{n \times d}$ is the encoder weight matrix, $\mathbf{b}_{\text{enc}} \in \mathbb{R}^n$ is a bias term, and $\mathbf{b}_{\text{pre}} \in \mathbb{R}^d$ normalizes the input. The decoder then reconstructs \mathbf{x} as:

$$\hat{\mathbf{x}} = \mathbf{W}_{\text{dec}} \mathbf{z} + \mathbf{b}_{\text{pre}}, \quad (2)$$

where $\mathbf{W}_{\text{dec}} \in \mathbb{R}^{d \times n}$ is the decoder weight matrix. To enforce sparsity, ℓ_1 norm with strength α is introduced as the regularization term, and the intact optimization objective is:

$$\mathcal{L}_{\text{SAE}} = \|\mathbf{x} - \hat{\mathbf{x}}\|_2^2 + \alpha \|\mathbf{z}\|_1. \quad (3)$$

In practice, instead of relying on ℓ_1 regularization, top- k Sparse Autoencoder [31] explicitly enforces the sparsity by using a **top- k selection** mechanism:

$$\mathbf{z} = \text{TopK}\left(\mathbf{W}_{\text{enc}}(\mathbf{x} - \mathbf{b}_{\text{pre}})\right), \quad (4)$$

where $\text{TopK}(\cdot)$ operator retains only the k highest-magnitude activations and zeroes out the rest. This modification ensures that only a fixed number of latent dimensions contribute to the reconstructed representation, making the extracted features more interpretable.

3.2 Visual Sparse Steering

In this section, we introduce **Visual Sparse Steering (VS2)**, a novel framework that leverages sparse features to steer neural representations toward meaningful semantic directions. Our approach targets two interconnected objectives, *i.e.*, (1) explicitly identifying semantically meaningful concepts embedded within latent representations and (2) utilizing these interpretable concepts to define steering directions that enhance downstream task performance by emphasizing relevant semantic information and reducing spurious correlations. Unlike standard steering methods that rely on explicitly curated positive and negative examples, our approach utilizes Sparse Autoencoders (SAEs) to automatically discover and isolate sparse concepts that assist in defining a steering direction. By selectively amplifying these concepts within the latent space, VS2 generates conceptually grounded steering vectors that improve model interpretability, enhance classification accuracy, and robustly mitigate reliance on superficial or irrelevant cues.

3.2.1 VS2: Visual Sparse Steering

Learning latent concept space. Given an input image $X \in \mathcal{X}$ and its corresponding embedding $\mathbf{x} \in \mathbb{R}^d$ extracted from layer i of a Vision Foundation Model (VFM), we define a *Concept Encoder* $E_c: \mathbb{R}^d \rightarrow \mathbb{R}^{|\mathcal{C}|}$ that maps the embedding \mathbf{x} into a sparse concept activation vector:

$$\mathbf{c} = E_c(\mathbf{x}) = (c_1, \dots, c_{|\mathcal{C}|}). \quad (5)$$

By imposing sparsity constraints described in Sec. 3.1 on the concept activations, the encoder E_c is encouraged to identify *disentangled*, semantically meaningful concepts. To map the concepts into the original representation space, we define a *Concept Decoder* $D_c: \mathbb{R}^{|\mathcal{C}|} \rightarrow \mathbb{R}^d$ that reconstructs the original embedding from these concepts:

$$\tilde{\mathbf{x}} = D_c(\mathbf{c}). \quad (6)$$

Since explicit supervision for concept identification is typically unavailable, we train the encoder-decoder pair jointly on training data \mathcal{X} , enforcing both sparsity and accurate embedding reconstruction to implicitly uncover meaningful concepts.

Constructing steering vector. At inference stage, emerged sparse concepts are deemed semantically significant and critical for downstream tasks, and we enhance them via a *Concept Upweighting Function* $U : \mathbb{R}^{|\mathcal{C}|} \rightarrow \mathbb{R}^{|\mathcal{C}|}$. In implementation, we simply scale the original concept activations \mathbf{c} by a factor of γ to amplify their effects:

$$\mathbf{c}' = U(\mathbf{c}) = \gamma \times \mathbf{c}. \quad (7)$$

Reconstructing this modified concept vector \mathbf{c}' provides a conceptually steered embedding:

$$\tilde{\mathbf{x}}' = D_c(\mathbf{c}'). \quad (8)$$

Since reconstruction steps inherently introduce approximation errors, we define the steering vector \mathbf{v} as:

$$\mathbf{v} = \tilde{\mathbf{x}}' - \tilde{\mathbf{x}}, \quad (9)$$

which explicitly represents the semantic shift induced by upweighting and mitigates the effects of the reconstruction errors.

Steer the target embedding. Obtaining the steering vector \mathbf{v} that aims to amplify the latent concepts embedded in \mathbf{x} , we shift the original embedding by adding the steering vector back as:

$$\hat{\mathbf{x}} = \mathbf{x} + \lambda \mathbf{v}. \quad (10)$$

where λ is a hyperparameter that controls the magnitude of steering. To stabilize the representation, we further rescale the ℓ_2 norm of the steered embedding to its original scale:

$$\hat{\mathbf{x}} = \frac{\hat{\mathbf{x}} \cdot \|\mathbf{x}\|_2}{\|\hat{\mathbf{x}}\|_2}. \quad (11)$$

Intuitively, this procedure precisely moves the embedding \mathbf{x} along directions defined by semantically relevant, interpretable concepts, thus improving interpretability and enhancing robustness against spurious correlations. We refer Fig. 1 (upper) for a schematic overview of VS2.

3.2.2 VS2⁺⁺: Visual Sparse Steering with Cached Data

In VS2, we leverage the learned SAEs to implicitly decide the critical concepts for a given latent embedding, and treat all identified concepts equally important. One natural speculation is that there are certain concepts that are unique and more important to the target underlying distribution, while others are more general even spuriously correlated. To this end, we propose VS2⁺⁺ that allows the access of cached training embedding at test-time to enable a more nuanced control over the concept steering.

Constructing Contrastive Groups. Given a query embedding \mathbf{x}_q and a cached dataset of embeddings $\{\mathbf{x}_i\}_{i=1}^M$, VS2⁺⁺ first retrieve the set of N nearest neighbors $\mathcal{N}_N(\mathbf{x}_q)$ for a query embedding \mathbf{x}_q is defined as:

$$\mathcal{N}_N(\mathbf{x}_q) = \underset{\substack{\{\mathbf{x}_i\} \subseteq \{\mathbf{x}_i\}_{i=1}^M \\ |\mathcal{N}_N(\mathbf{x}_q)|=N}}{\arg \max} S(\mathbf{x}_q, \mathbf{x}_i), \quad (12)$$

where $S(\cdot)$ denotes the measurement of cosine similarity.

After retrieving $\mathcal{N}_N(\mathbf{x}_q)$, we obtain the pseudo-label for the query embedding $\hat{y}_q = \arg \max_y P(y | \mathbf{x}_q)$, where $P(y | \mathbf{x})$ is the classifier’s predicted probability for label y . Similarly, for each neighbor $\mathbf{x}_i \in \mathcal{N}_N(\mathbf{x}_q)$, we compute its pseudo-label: $\hat{y}_i = \arg \max_y P(y | \mathbf{x}_i)$.

We then construct the *positive* group, $\mathbb{S}^+(\mathbf{x}_q)$, by selecting neighbors sharing the same pseudo-label as the query embedding:

$$\mathbb{S}^+(\mathbf{x}_q) = \{\mathbf{x}_i \in \mathcal{N}_N(\mathbf{x}_q) \mid \hat{y}_i = \hat{y}_q\}. \quad (13)$$

Likewise, the *negative* group, $\mathbb{S}^-(\mathbf{x}_q)$, is formed by the remaining neighbors:

$$\mathbb{S}^-(\mathbf{x}_q) = \mathcal{N}_N(\mathbf{x}_q) \setminus \mathbb{S}^+(\mathbf{x}_q). \quad (14)$$

Table 1: Benchmarking Visual Sparse Steering: Zero-Shot Accuracy (%) with and Without External Data on CIFAR-100, CUB-200, and Tiny Imagenet using ViT-B/32 and ViT-B/16.

Method	CIFAR-100		CUB-200		Tiny-IN	
	ViT-B/32	ViT-B/16	ViT-B/32	ViT-B/16	ViT-B/32	ViT-B/16
Zero-shot (no retrieval)						
CLIP _{ZS}	61.07 (0)	63.96 (0)	51.76 (0)	55.06 (0)	56.64 (0)	61.08 (0)
SAE _{REC} ^A	58.01 (-3.06)	64.05 (+0.09)	47.45 (-4.31)	51.81 (-3.25)	30.56 (-26.08)	52.96 (-8.12)
SAE _{REC} ^F	58.22 (-2.85)	63.42 (-0.54)	48.08 (-3.68)	51.43 (-3.63)	36.33 (-20.31)	54.84 (-6.24)
SAE _{REC} ^{F+γ}	62.69 (+1.62)	66.81 (+2.85)	49.41 (-2.35)	53.28 (-1.78)	39.49 (-17.15)	58.81 (-2.27)
VS2 (ours)	64.52 (+3.45)	68.08 (+4.12)	52.69 (+0.93)	56.14 (+1.08)	58.14 (+1.50)	62.92 (+1.84)
VS2 + PASS (ours)	70.64 (+9.57)	68.23 (+4.27)	52.97 (+1.21)	56.63 (+1.57)	57.94 (+1.30)	62.98 (+1.90)
RAG-enhanced (oracle cache)						
Weighted RAG	76.43 (+15.36)	69.78 (+5.82)	58.32 (+6.56)	60.65 (+5.59)	72.53 (+15.89)	67.84 (+6.75)
CLIP Steering Vector	81.85 (+20.78)	84.12 (+20.16)	56.42 (+4.66)	61.51 (+6.45)	80.38 (+23.74)	84.07 (+22.99)
VS2++	81.95 (+20.88)	85.40 (+21.44)	58.84 (+7.08)	61.91 (+6.85)	73.27 (+16.63)	81.55 (+20.47)
RAG-enhanced (non-oracle cache)						
CLIP Steering Vector	77.22 (+16.15)	78.97 (+15.01)	47.89 (-3.87)	53.95 (-1.11)	74.06 (+17.42)	76.79 (+15.71)
VS2++	77.11 (+16.04)	79.14 (+15.18)	52.81 (+1.05)	57.02 (+1.96)	72.12 (+15.48)	76.92 (+15.84)

Selective Steering. For each embedding $\mathbf{x}_i \in \mathbb{S}^+(\mathbf{x}_q)$, VS2⁺⁺ first applies VS2 (Eq. 7,8,9) to acquire a directional vector \mathbf{v}_i^p that underscores the underlying concepts within the given embedding. We repeat the same procedure for each $\mathbf{x}_j \in \mathbb{S}^-(\mathbf{x}_q)$ to obtain the negative steering vectors \mathbf{v}_j^n . We then average these per-embedding steering vectors within each group, yielding the *positive anchor*

$$\bar{\mathbf{v}}^p = \frac{1}{|\mathbb{S}^+(\mathbf{x}_q)|} \sum_{\mathbf{x}_i \in \mathbb{S}^+(\mathbf{x}_q)} \mathbf{v}_i^p, \quad (15)$$

and the *negative anchor*

$$\bar{\mathbf{v}}^n = \frac{1}{|\mathbb{S}^-(\mathbf{x}_q)|} \sum_{\mathbf{x}_j \in \mathbb{S}^-(\mathbf{x}_q)} \mathbf{v}_j^n. \quad (16)$$

Finally, we obtain the *contrastive steering vector* by subtracting the negative anchor from the positive anchor:

$$\mathbf{v} = \bar{\mathbf{v}}^p - \bar{\mathbf{v}}^n, \quad (17)$$

and apply it to the query embedding \mathbf{x}_q in the same manner as VS2:

$$\hat{\mathbf{x}}_q = \mathbf{x}_q + \lambda \mathbf{v}, \quad \hat{\mathbf{x}}_q = \frac{\hat{\mathbf{x}}_q \cdot \|\mathbf{x}_q\|_2}{\|\hat{\mathbf{x}}_q\|_2}. \quad (18)$$

This selective scheme thus anchors the steering directions in concepts consistently activated within the positive group, while suppressing undesired features highlighted by the negative group. Since VS2⁺⁺ retrieves N-nearest embeddings of a query to construct both positive and negative groups, negative group contains non-trivial hard cases.

4 Experiments

Experimental Setup. We test VS2 and VS2⁺⁺ on CIFAR-100 [46], Tiny-ImageNet [47], and CUB-200 [48] three datasets, covering standard, complex, and fine-grained classification tasks. These datasets vary in scale, diversity, and class distribution, allowing us to assess VS2 and VS2⁺⁺ in both general and imbalanced classification scenarios. For vision foundation model, we use CLIP [18] with ViT-B/32, and ViT-B/16 backbones. We train top- k Sparse Autoencoders (SAEs) on the CLS token embeddings extracted from every layer of CLIP’s vision transformer, using the training data of each dataset to learn sparse latent representations. More details regarding the training of the top- k Sparse Autoencoders can be found in the Appendix C.

4.1 Visual Sparse Steering methods

4.1.1 VS2: Visual Sparse Steering without Contrastive Data

Baselines. We evaluate the effectiveness of VS2 in the absence of external contrastive data. As baselines, we report: (1) the zero-shot performance of the original CLIP model (CLIP_{ZS}); (2)

CLIP_{REC}^F, which uses the SAE-reconstructed CLS token from the final layer without any steering; and (3) CLIP_{REC}^A, which uses the reconstructed CLS tokens from all layers. These baselines isolate the effect of reconstruction alone, without applying any modification or steering vector. All top- k SAEs are trained on CLS token representations across all transformer layers. In addition to these baselines, we report SAE_{REC}^{F+ γ} that applies steering by upweighting the top- k sparse features of the reconstructed CLS token of the final layer with a scaling factor of $\gamma = 1.5$. This variant isolates the impact of steering the SAE’s latent activations by amplifying their top- k before the CLS embedding is reconstructed, letting us quantify the benefit attributable to this targeted up-weighting alone. In Appendix G, we provide the pseudocode for main differences between the proposed baselines and VS2. In Appendix H, we also provide comparative results of our method compared to other baselines such as Splice [16]. Note that Splice uses an external vocabulary to construct latent features; in contrast, we use unsupervised SAEs to learn latent features for VS2 and VS2⁺⁺.

Results. From Table 1, we demonstrate that using only SAE reconstructions generally reduces zero-shot performance in all datasets; we hypothesize this is due to reconstruction errors in SAEs [49]. However, when SAE features are amplified in the reconstruction, performance can improve, as demonstrated by SAE_{REC}^{F+ γ} for CIFAR-100. Specifically, SAE_{REC}^{F+ γ} outperforms the zero-shot baseline on CIFAR-100 by 1.62% and 2.85% using the ViT-B/32 and ViT-B/16 backbones respectively. However, SAE_{REC}^{F+ γ} is worse than the CLIP baseline on CUB-200 and Tiny-ImageNet. In contrast, **our method VS2 consistently outperforms all baseline methods across all datasets and ViT backbones**, surpassing zero-shot CLIP by 3.45% and 4.12% on CIFAR-100, 0.93% and 1.08% on CUB-200, and 1.50% and 1.84% on Tiny-ImageNet with ViT-B/32 and ViT-B/16 backbones, respectively. **In summary, we demonstrate that our proposed steering vectors using SAEs can improve downstream classification performance on vision tasks without relying on any external data or supervision.** In Appendix A, we also provide evidence that the sparse features are interpretable; they can capture subtle class-specific attributes and concepts such as birds with gray upperpart, white underpart, white-colored throat and black eyes. Finally, in Appendix B, we provide a sensitivity analysis of VS2 hyperparameters γ and λ showing the robustness of our proposed methods.

4.1.2 VS2⁺⁺: Visual Sparse Steering with Selectively Amplifying Features

In VS2, we leverage learned SAEs to identify critical concepts from a latent embedding, treating all activated concepts as equally important. However, some concepts may be more discriminative or unique to the target class, while others may be generic or even spuriously correlated with a class label. To enable finer control over concept importance, we introduce VS2⁺⁺, which accesses cached training data at test time to guide steering more selectively. As a proxy for identifying salient features, we adopt a Retrieval-Augmented Generation (RAG) approach: we retrieve the top-50 most similar training images to the test input using DINOv2 [50] and average their sparse activations. To construct the positive and negative sets as shown in equations 13, 14, we assign pseudolabels using a CLIP classifier; images with the most frequent pseudolabel form the positive set, while the remaining images serve as negatives. This setup corresponds to the Non-oracle cache in Table 1. For comparison, we also report an unrealistic scenario that serves as an upper-bound *i.e.* Oracle cache setting that uses ground-truth labels to define positives and negatives.

Baselines. As a baseline in the Retrieval-Augmented Generation (RAG) pipeline [51], we combine the test query embedding with a weighted aggregation of retrieved document embeddings. Additional details on the weighting strategy are provided in Appendix D. We also include a non-SAE variant that constructs a steering vector by averaging the CLIP embeddings of the positive and negative sets and taking their difference, yielding a purely contrastive direction without relying on Sparse Autoencoders.

Results. In Table 1, we present the results for VS2 ++ when external data is available under both RAG-enhanced settings where we have oracle and non-oracle cache data. When we have oracle positive and negative sets, we observe that VS2⁺⁺ surpasses all other methods under almost every setting. Weighted RAG performs worse than the steering vector approaches (both CLIP and VS2⁺⁺), suggesting that directionality is more informative than proximity. In the more realistic scenario where we do not have oracle positive and negative sets, we observe drops in accuracies. We hypothesize that this degradation is due to inaccuracies in pseudolabeling, resulting in the amplification of spurious

Table 2: **Top-10 class gains on CIFAR-100**. Numbers are top-1 accuracies; green = absolute gain over zero-shot (ZS).

(a) VS2					(b) VS2++				
Class	ZS	VS2 (+ Δ)	Mislabel	Why visually confusing	Class	ZS	VS2++ (+ Δ)	Mislabel	Why visually confusing
tractor	55.0	80.0 $\uparrow(+25.0)$	lawn_mower	Both are wheeled agricultural machines; similar viewed side-on.	spider	53.0	91.0 $\uparrow(+38.0)$	bee	Small multi-legged insects; dark radial silhouettes.
forest	35.0	58.0 $\uparrow(+23.0)$	pine_tree	Dense tree canopies often dominated by tall conifers.	tiger	48.0	84.0 $\uparrow(+36.0)$	lion	Large orange/brown big cats; stripes vs. mane often unclear at low resolution.
man	53.0	74.0 $\uparrow(+21.0)$	boy	Male human silhouette; age difference subtle at CIFAR resolution.	flatfish	49.0	85.0 $\uparrow(+36.0)$	whale	Flattened marine shapes against blue water backgrounds.
bus	51.0	68.0 $\uparrow(+17.0)$	pickup_truck	Rectangular vehicle profile with windows and wheels.	possum	30.0	65.0 $\uparrow(+35.0)$	hamster	Small brown furry mammals with rounded bodies.
snake	61.0	76.0 $\uparrow(+15.0)$	worm	Long, legless bodies with smooth textures.	lizard	39.0	74.0 $\uparrow(+35.0)$	snake	Slender reptiles; legs on lizard hard to spot in 32×32 images.
woman	57.0	71.0 $\uparrow(+14.0)$	girl	Female human figures; height/size cues are small.	sweet_pepper	58.0	92.0 $\uparrow(+34.0)$	orange	Round orange-coloured produce with glossy skins.
trout	18.0	32.0 $\uparrow(+14.0)$	aquarium_fish	Similar fish shape and reflective scales in water scenes.	raccoon	49.0	83.0 $\uparrow(+34.0)$	skunk	Mid-sized nocturnal mammals with dark fur and contrasting markings.
cockroach	49.0	62.0 $\uparrow(+13.0)$	beetle	Small, dark exoskeleton insects with segmented bodies.	shrew	46.0	79.0 $\uparrow(+33.0)$	skunk	Small ground mammals; dark elongated silhouettes blur distinguishing cues.
bridge	72.0	83.0 $\uparrow(+11.0)$	sea	Large spans photographed above wide blue water areas.	snail	53.0	86.0 $\uparrow(+33.0)$	mushroom	Brown dome (shell vs. cap) resting on the forest floor.
rose	58.0	68.0 $\uparrow(+10.0)$	poppy	Red, multi-petal flowers with central dark core.	beetle	49.0	82.0 $\uparrow(+33.0)$	cockroach	Dark, shiny exoskeletal insects with similar body shapes.

directions in the SAE latent space. However, across the six configurations, VS2⁺⁺ outperforms the CLIP Steering Vector in four cases and falls behind only in the ViT-B/32 runs for CIFAR-100 and Tiny-ImageNet (with CIFAR-100 essentially on par). These results suggest that there remains significant room for improvement in actively selecting which sparse features to steer, especially under noisy or weakly supervised retrieval scenarios. In Appendix I, we conduct ablation studies on the top- N retrieved images that indicate that the utility of neighbor-based aggregation is dataset-dependent: general object recognition tasks benefit from larger N , while fine-grained classification may require more careful control of retrieval scope.

4.1.3 Fine-Grained Per-Class Accuracy Analysis

To understand *where* Visual Sparse Steering helps most, we compute per-class top-1 accuracy on CIFAR-100 with a ViT-B/32 backbone and report the ten largest improvements in Table 2. The results reveal a long-tailed pattern: **VS2 lifts accuracy by up to 25 % in individual classes (e.g. *lawn-mower* \rightarrow *tractor*, *pine-tree* \rightarrow *forest*)**, while **VS2++ reaches gains of 38 %** when high-quality neighbours are available (e.g. *bee* \rightarrow *spider*, *lion* \rightarrow *tiger*, *whale* \rightarrow *flatfish*). In all cases, the corrected predictions involve visually or taxonomically proximate categories, indicating that sparse steering primarily *disambiguates* fine-grained confusions rather than providing a uniform boost. This behaviour aligns with our qualitative findings in the Appendix A.2, where the top- k SAE features capture subtle class-specific attributes (birds with gray upperpart, white underpart, white-colored throat and black eyes *etc.*) that are otherwise entangled in the original CLIP embedding. A more detailed list of per-class performance accuracies of VS2 and VS2⁺⁺ is provided in Table 9 in the Appendix.

4.2 Prototype-Aware Sparse Steering Vectors

Our core methods, VS2 and its retrieval-augmented variant VS2⁺⁺, enhance zero-shot classification by steering CLIP embeddings along directions identified by a top- k Sparse Autoencoder (SAE). These directions correspond to latent *concepts* that, ideally, align with class-discriminative features. Steering in these directions upweights what the model has learned to be important during reconstruction. This raises a central hypothesis: **the reconstruction task itself is to some extent sufficient to uncover features that are also relevant for classification**. In other words, there is a meaningful overlap between features that are important for reconstructing the CLS token and those that are predictive for the downstream task. In this section, drawing inspiration from prototype theory [52], we investigate whether incorporating prototype information during SAE training can better align the features important for reconstruction with those that are critical for downstream classification.

The limited improvements observed on fine-grained datasets like CUB-200 and Tiny-ImageNet suggest that the challenge lies not just in identifying sparse features, but in uncovering the *correct* ones. This shifts the central question from “What are the most important sparse features to select?” to a deeper inquiry: “Can the reconstruction objective alone reliably capture features that are most useful for classification and if not, how can task-relevant information be effectively incorporated?”

Oracle steering with known prototypes. Following prototype theory, we collect for every class the ten images that ViT-B/32 CLIP classifies with the highest confidence; these serve as *oracle prototypes*. Given the true class label y , we build a prototype steering vector by averaging their latent sparse features. **VS2 using oracle prototypes can lift CLIP to 97.5% on CIFAR-100, 91.04% on CUB-200, and 90.1% on Tiny-ImageNet.** This confirms the existence of discriminative sparse directions. In Appendix E we further examine the discriminative ability (measured by orthogonality) of these steering vectors. Generally, these prototype vectors have a low cosine similarity, yet a non-negligible tail reveals strongly overlapping directions between visually or semantically close categories.

Prototype-aligned SAE (PASS). Above, we constructed steering vectors using the pretrained SAE features of oracle prototypes. Now, we consider whether prototypes can be used to learn new, more informative SAE features. We assume during SAE training that we have access to class labels. Then, to the SAE loss we add a regularization term which encourages SAE features to be close to their class mean. That is, for a training sample i with latent sparse feature \mathbf{z}_i and class mean $\bar{\mathbf{z}}_{\text{class}(i)}$ we minimize

$$\mathcal{L} = \mathcal{L}_{\text{recon}} + w_{\text{aux}} \|\mathbf{z}_i - \bar{\mathbf{z}}_{\text{class}(i)}\|_2^2, \quad (19)$$

where w_{aux} controls the strength of the prototype-alignment term relative to the reconstruction loss and is set to 0.8. We refer to the resulting steering method as **PASS** (Prototype-Aligned Sparse Steering). Although PASS uses class labels during SAE training, it remains *fully test-time unsupervised*. Empirically, in Table 1, we observe that PASS outperforms VS2 across all datasets, with particularly substantial gains on CIFAR-100. However, this improvement comes at the cost of requiring labels for each training sample during SAE training. Gains are modest on CUB-200 and Tiny-ImageNet, and we thus hypothesize that classes which share many features require richer or multi-prototype guidance which is an intriguing avenue for future work.

5 Conclusion

We introduce Visual Sparse Steering VS2 and its retrieval-augmented variant VS2⁺⁺, two test-time methods that steer vision foundation models using sparse features obtained from top- k Sparse Autoencoders without requiring contrastive data. Specifically, VS2 consistently outperforms all baseline methods across all datasets and ViT backbones, surpassing zero-shot CLIP by 3.45% and 4.12% on CIFAR-100, 0.93% and 1.08% on CUB-200, and 1.50% and 1.84% on Tiny-ImageNet with ViT-B/32 and ViT-B/16 backbones, respectively. To control concept importance more precisely, we propose VS2⁺⁺. With oracle positive/negative sets, VS2⁺⁺ surpasses every baseline in nearly every configuration, achieving absolute top-1 gains over CLIP zero-shot of up to 21.44% on CIFAR-100, 7.08% on CUB-200, and 20.47% on Tiny-ImageNet. When those sets are noisy, its accuracy drops but still surpasses the standard Steering Vector in most cases, highlighting the need for better feature selection under weakly supervised retrieval. Interestingly, VS2 and VS2⁺⁺ raise per-class accuracy by up to 25% and 38%, respectively, showing that sparse steering benefits specific classes by disambiguating visually or taxonomically proximate categories rather than providing a uniform boost. Finally, to further align the sparse features learned through the SAE reconstruction task with those important for downstream performance, we proposed Prototype-Aligned Sparse Steering (PASS). By adding a lightweight prototype-alignment loss during SAE training (labels used only in training, still test-time unsupervised) PASS consistently, though slightly, outperforms VS2, offering a marginal 6.12% gain over VS2 only on CIFAR-100 with ViT-B/32. Selecting appropriate prototypes or exploring multi-prototype guidance is an intriguing avenue for future work.

References

- [1] Alec Radford, Jong Wook Kim, Chris Hallacy, Aditya Ramesh, Gabriel Goh, Sandhini Agarwal, Girish Sastry, Amanda Askell, Pamela Mishkin, Jack Clark, et al. Learning transferable visual models from natural language supervision. In *International conference on machine learning*, pages 8748–8763. PmLR, 2021.
- [2] Alexander Kirillov, Eric Mintun, Nikhila Ravi, Hanzi Mao, Chloe Rolland, Laura Gustafson, Tete Xiao, Spencer Whitehead, Alexander C Berg, Wan-Yen Lo, et al. Segment anything. In *Proceedings of the IEEE/CVF international conference on computer vision*, pages 4015–4026, 2023.
- [3] Hugo Touvron, Louis Martin, Kevin Stone, Peter Albert, Amjad Almahairi, Yasmine Babaei, Nikolay Bashlykov, Soumya Batra, Prajjwal Bhargava, Shruti Bhosale, et al. Llama 2: Open foundation and fine-tuned chat models. *arXiv preprint arXiv:2307.09288*, 2023.
- [4] Haotian Liu, Chunyuan Li, Qingyang Wu, and Yong Jae Lee. Visual instruction tuning. *Advances in neural information processing systems*, 36:34892–34916, 2023.
- [5] Josh Achiam, Steven Adler, Sandhini Agarwal, Lama Ahmad, Ilge Akkaya, Florencia Leoni Aleman, Diogo Almeida, Janko Altenschmidt, Sam Altman, Shyamal Anadkat, et al. Gpt-4 technical report. *arXiv preprint arXiv:2303.08774*, 2023.
- [6] Shengyu Zhang, Linfeng Dong, Xiaoya Li, Sen Zhang, Xiaofei Sun, Shuhe Wang, Jiwei Li, Runyi Hu, Tianwei Zhang, Fei Wu, et al. Instruction tuning for large language models: A survey. *arXiv preprint arXiv:2308.10792*, 2023.
- [7] Guanting Dong, Hongyi Yuan, Keming Lu, Chengpeng Li, Mingfeng Xue, Dayiheng Liu, Wei Wang, Zheng Yuan, Chang Zhou, and Jingren Zhou. How abilities in large language models are affected by supervised fine-tuning data composition. *arXiv preprint arXiv:2310.05492*, 2023.
- [8] Brian Lester, Rami Al-Rfou, and Noah Constant. The power of scale for parameter-efficient prompt tuning. *arXiv preprint arXiv:2104.08691*, 2021.
- [9] Edward J Hu, Yelong Shen, Phillip Wallis, Zeyuan Allen-Zhu, Yuanzhi Li, Shean Wang, Lu Wang, Weizhu Chen, et al. Lora: Low-rank adaptation of large language models. *ICLR*, 1(2):3, 2022.
- [10] Haokun Liu, Derek Tam, Mohammed Muqeeth, Jay Mohta, Tenghao Huang, Mohit Bansal, and Colin A Raffel. Few-shot parameter-efficient fine-tuning is better and cheaper than in-context learning. *Advances in Neural Information Processing Systems*, 35:1950–1965, 2022.
- [11] Alexander Matt Turner, Lisa Thiergart, David Udell, Gavin Leech, Ulisse Mini, and Monte MacDiarmid. Activation addition: Steering language models without optimization, 2023.
- [12] Andy Zou, Long Phan, Sarah Chen, James Campbell, Phillip Guo, Richard Ren, Alexander Pan, Xuwang Yin, Mantas Mazeika, Ann-Kathrin Dombrowski, Shashwat Goel, Nathaniel Li, Michael J. Byun, Zifan Wang, Alex Mallen, Steven Basart, Sanmi Koyejo, Dawn Song, Matt Fredrikson, J. Zico Kolter, and Dan Hendrycks. Representation engineering: A top-down approach to ai transparency, 2023.
- [13] Sheng Liu, Haotian Ye, Lei Xing, and James Zou. In-context vectors: Making in context learning more effective and controllable through latent space steering, 2024.
- [14] Hugofry. Towards multimodal interpretability: Learning sparse interpretable features in vision transformers. *LessWrong*, April 29 2024.
- [15] G. Daujotas. Interpreting and steering features in images. *LessWrong*, June 20 2024.
- [16] Usha Bhalla, Alex Oesterling, Suraj Srinivas, Flavio Calmon, and Himabindu Lakkaraju. Interpreting clip with sparse linear concept embeddings (splice). *Advances in Neural Information Processing Systems*, 37:84298–84328, 2024.
- [17] Samuel Stevens, Wei-Lun Chao, Tanya Berger-Wolf, and Yu Su. Sparse autoencoders for scientifically rigorous interpretation of vision models. *arXiv preprint arXiv:2502.06755*, 2025.

- [18] Alec Radford, Jong Wook Kim, Chris Hallacy, Aditya Ramesh, Gabriel Goh, Sandhini Agarwal, Girish Sastry, Amanda Askell, Pamela Mishkin, Jack Clark, et al. Learning transferable visual models from natural language supervision. In *International conference on machine learning*, pages 8748–8763. PmLR, 2021.
- [19] Karen Simonyan, Andrea Vedaldi, and Andrew Zisserman. Visualising image classification models and saliency maps. *Deep Inside Convolutional Networks*, 2(2), 2014.
- [20] Matthew D Zeiler and Rob Fergus. Visualizing and understanding convolutional networks. In *Computer Vision—ECCV 2014: 13th European Conference, Zurich, Switzerland, September 6–12, 2014, Proceedings, Part I 13*, pages 818–833. Springer, 2014.
- [21] Chris Olah, Alexander Mordvintsev, and Ludwig Schubert. Feature visualization. *Distill*, 2(11):e7, 2017.
- [22] David Bau, Bolei Zhou, Aditya Khosla, Aude Oliva, and Antonio Torralba. Network dissection: Quantifying interpretability of deep visual representations. In *Proceedings of the IEEE conference on computer vision and pattern recognition*, pages 6541–6549, 2017.
- [23] Tuomas Oikarinen and Tsui-Wei Weng. Clip-dissect: Automatic description of neuron representations in deep vision networks. *arXiv preprint arXiv:2204.10965*, 2022.
- [24] Nelson Elhage, Neel Nanda, Catherine Olsson, Tom Henighan, Nicholas Joseph, Ben Mann, Amanda Askell, Yuntao Bai, Anna Chen, Tom Conerly, et al. A mathematical framework for transformer circuits. *Transformer Circuits Thread*, 1(1):12, 2021.
- [25] Chris Olah, Nick Cammarata, Ludwig Schubert, Gabriel Goh, Michael Petrov, and Shan Carter. Zoom in: An introduction to circuits. *Distill*, 5(3):e00024–001, 2020.
- [26] Nelson Elhage, Tristan Hume, Catherine Olsson, Nicholas Schiefer, Tom Henighan, Shauna Kravec, Zac Hatfield-Dodds, Robert Lasenby, Dawn Drain, Carol Chen, et al. Toy models of superposition. *arXiv preprint arXiv:2209.10652*, 2022.
- [27] Lee Sharkey, Dan Braun, and Beren Millidge. Taking features out of superposition with sparse autoencoders. In *AI Alignment Forum*, volume 8, pages 15–16, 2022.
- [28] Trenton Bricken, Adly Templeton, Joshua Batson, Brian Chen, Adam Jermyn, Tom Conerly, Nick Turner, Cem Anil, Carson Denison, Amanda Askell, Robert Lasenby, Yifan Wu, Shauna Kravec, Nicholas Schiefer, Tim Maxwell, Nicholas Joseph, Zac Hatfield-Dodds, Alex Tamkin, Karina Nguyen, Brayden McLean, Josiah E Burke, Tristan Hume, Shan Carter, Tom Henighan, and Christopher Olah. Towards monosemanticity: Decomposing language models with dictionary learning. *Transformer Circuits Thread*, 2023. <https://transformer-circuits.pub/2023/monosemantic-features/index.html>.
- [29] Adly Templeton. *Scaling monosemanticity: Extracting interpretable features from claude 3 sonnet*. Anthropic, 2024.
- [30] Hoagy Cunningham, Aidan Ewart, Logan Riggs, Robert Huben, and Lee Sharkey. Sparse autoencoders find highly interpretable features in language models. *arXiv preprint arXiv:2309.08600*, 2023.
- [31] Leo Gao, Tom Dupré la Tour, Henk Tillman, Gabriel Goh, Rajan Troll, Alec Radford, Ilya Sutskever, Jan Leike, and Jeffrey Wu. Scaling and evaluating sparse autoencoders. *arXiv preprint arXiv:2406.04093*, 2024.
- [32] Shruti Joshi, Andrea Dittadi, Sébastien Lachapelle, and Dhanya Sridhar. Identifiable steering via sparse autoencoding of multi-concept shifts. *arXiv preprint arXiv:2502.12179*, 2025.
- [33] Thomas Fel, Ekdeep Singh Lubana, Jacob S Prince, Matthew Kowal, Victor Boutin, Isabel Papadimitriou, Binxu Wang, Martin Wattenberg, Demba Ba, and Talia Konkle. Archetypal sae: Adaptive and stable dictionary learning for concept extraction in large vision models. *arXiv preprint arXiv:2502.12892*, 2025.

- [34] Harrish Thasarathan, Julian Forsyth, Thomas Fel, Matthew Kowal, and Konstantinos Derpanis. Universal sparse autoencoders: Interpretable cross-model concept alignment. *arXiv preprint arXiv:2502.03714*, 2025.
- [35] Sonia Joseph, Praneet Suresh, Ethan Goldfarb, Lorenz Hufe, Yossi Gandelsman, Robert Graham, Danilo Bzdok, Wojciech Samek, and Blake Aaron Richards. Steering clip’s vision transformer with sparse autoencoders. *arXiv preprint arXiv:2504.08729*, 2025.
- [36] Hyesu Lim, Jinho Choi, Jaegul Choo, and Steffen Schneider. Sparse autoencoders reveal selective remapping of visual concepts during adaptation. *arXiv preprint arXiv:2412.05276*, 2024.
- [37] Kiho Park, Yo Joong Choe, and Victor Veitch. The linear representation hypothesis and the geometry of large language models. In *Causal Representation Learning Workshop at NeurIPS 2023*, 2023.
- [38] Evan Hernandez, Arnab Sen Sharma, Tal Haklay, Kevin Meng, Martin Wattenberg, Jacob Andreas, Yonatan Belinkov, and David Bau. Linearity of relation decoding in transformer language models. In *The Twelfth International Conference on Learning Representations*, 2024.
- [39] Tomas Mikolov, Ilya Sutskever, Kai Chen, Greg S Corrado, and Jeff Dean. Distributed representations of words and phrases and their compositionality. In C.J. Burges, L. Bottou, M. Welling, Z. Ghahramani, and K.Q. Weinberger, editors, *Advances in Neural Information Processing Systems*, volume 26. Curran Associates, Inc., 2013.
- [40] Kenneth Li, Oam Patel, Fernanda Viégas, Hanspeter Pfister, and Martin Wattenberg. Inference-time intervention: Eliciting truthful answers from a language model. In A. Oh, T. Neumann, A. Globerson, K. Saenko, M. Hardt, and S. Levine, editors, *Advances in Neural Information Processing Systems*, volume 36, pages 41451–41530. Curran Associates, Inc., 2023.
- [41] Zhuowei Li, Haizhou Shi, Yunhe Gao, Di Liu, Zhenting Wang, Yuxiao Chen, Ting Liu, Long Zhao, Hao Wang, and Dimitris N. Metaxas. The hidden life of tokens: Reducing hallucination of large vision-language models via visual information steering, 2025.
- [42] Zhuowei Li, Zihao Xu, Ligong Han, Yunhe Gao, Song Wen, Di Liu, Hao Wang, and Dimitris N. Metaxas. Implicit in-context learning. In *The Thirteenth International Conference on Learning Representations*, 2025.
- [43] Paul Gavrikov, Jovita Lukasik, Steffen Jung, Robert Geirhos, Muhammad Jehanzeb Mirza, Margret Keuper, and Janis Keuper. Can we talk models into seeing the world differently? In *Thirteenth International Conference on Learning Representations*. OpenReview. net, 2025.
- [44] Reza Bayat, Ali Rahimi-Kalahroudi, Mohammad Pezeshki, Sarath Chandar, and Pascal Vincent. Steering large language model activations in sparse spaces. *arXiv preprint arXiv:2503.00177*, 2025.
- [45] Aleksandar Makelov. Sparse autoencoders match supervised features for model steering on the ioi task. In *ICML 2024 Workshop on Mechanistic Interpretability*, 2024.
- [46] Alex Krizhevsky, Geoffrey Hinton, et al. Learning multiple layers of features from tiny images. 2009.
- [47] Yann Le and Xuan Yang. Tiny imagenet visual recognition challenge. *CS 231N*, 7(7):3, 2015.
- [48] Catherine Wah, Steve Branson, Peter Welinder, Pietro Perona, and Serge Belongie. The caltech-ucsd birds-200-2011 dataset. 2011.
- [49] Joshua Engels, Logan Riggs Smith, and Max Tegmark. Decomposing the dark matter of sparse autoencoders. *Transactions on Machine Learning Research*, 2025.
- [50] Maxime Oquab, Timothée Darcet, Théo Moutakanni, Huy Vo, Marc Szafraniec, Vasil Khalidov, Pierre Fernandez, Daniel Haziza, Francisco Massa, Alaaeldin El-Nouby, et al. Dinov2: Learning robust visual features without supervision. *arXiv preprint arXiv:2304.07193*, 2023.

- [51] Patrick Lewis, Ethan Perez, Aleksandra Piktus, Fabio Petroni, Vladimir Karpukhin, Naman Goyal, Heinrich Küttler, Mike Lewis, Wen-tau Yih, Tim Rocktäschel, et al. Retrieval-augmented generation for knowledge-intensive nlp tasks. *Advances in neural information processing systems*, 33:9459–9474, 2020.
- [52] Eleanor H Rosch. Natural categories. *Cognitive psychology*, 4(3):328–350, 1973.
- [53] EleutherAI. Sparsify: Sparse autoencoder library. <https://github.com/EleutherAI/sparsify>, 2024. GitHub repository, commit <commit-hash>, accessed May 16 2025.

Appendix

A Decoding the Sparse Latent Space: Insights from SAEs

Our proposed methods, VS2 and VS2⁺⁺, achieve significant classification performance gains, primarily due to the contribution of Sparse Autoencoders (SAEs). We hypothesize that SAEs identify meaningful sparse concepts, which in turn guide the steering mechanisms. To validate this assumption, we conduct both quantitative and qualitative evaluations to assess the significance of the learned concepts.

A.1 Quantitative Evaluation of Concept Significance.

To further evaluate the role of interpretable sparse features, we manipulate the top- k most active latent dimensions extracted via Sparse Autoencoders. This experiment examines whether these features are critical for classification and how model predictions change under different modifications. We explore the following manipulation settings:

1. **Zeroing-Out** ($\gamma = 0$): We set the top- k most active features to zero before applying the steering vector. This removes their influence while preserving the remaining latent structure.
2. **Negation** ($\gamma = -1$): We invert the sign of the top- k features before applying the steering vector, effectively pushing the representation in the opposite direction. This tests whether these dimensions encode class-discriminative information.

Table 3 reports the zero-shot classification accuracy of $\text{SAE}_{\text{REC}}^{\text{F}+\gamma}$ using ViT-B/32 after applying these transformations to the Sparse Steering vector intervention. **We observe that negating or zeroing the top- k most important concepts consistently degrades performance across all datasets.** This result confirms that the concepts learned by the Sparse Autoencoders are essential for classification.

Table 3: **Effect of manipulating top- k sparse codes.** Zero-shot accuracy (%) drops sharply when dominant sparse features are zeroed ($\gamma = 0$) or negated ($\gamma = -1$), confirming their importance.

Modification	CIFAR-100	CUB-200	Tiny-IN
CLIP _{ZS}	61.07	38.68	56.64
$\text{SAE}_{\text{REC}}^{\text{F}+\gamma}$	62.69	37.30	39.49
+ <i>Zero-out</i> ($\gamma = 0$)	1.71	1.14	16.11
+ <i>Negate</i> ($\gamma = -1$)	0.06	0.00	0.82

A.2 Qualitative Evaluation of Concept Significance.

We qualitatively investigate the concepts learned in the sparse latent representations of the top- k activations in the Sparse Autoencoder (SAE). Specifically, we assess the learned features by analyzing feature activations for each input and identifying the inputs that exhibit the highest activations for a given feature. Unlike mechanistic interpretability in the language domain, where an LLM can be used to assign semantic labels to a feature by summarizing its highly activated inputs, the vision domain lacks an equivalent automated labeling process.

To avoid reliance on human qualitative evaluation, we leverage annotated datasets where each image is associated with predefined attributes. For the qualitative evaluation of concept significance, we use the CUB dataset, which provides rich concept annotations for each image, enabling a structured assessment of the learned representations. Specifically, we investigate whether we can identify specific latent features with the highest **concept coverage** among their top- k most activated images. Concept coverage refers to how consistently a specific interpretable concept (e.g., an identifiable object category, attribute, or semantic idea) appears across a set of highly activated examples for a given SAE dimension. The intuition is that if a specific concept frequently emerges among the top-activating images for a particular dimension, that dimension is strongly associated with that concept.

For feature 511 as shown in Figure 2 (left), the activated images exhibit consistent semantic characteristics, including a gray upper part and a white underpart. Notably, this feature predominantly

activates for images from similar but different classes, specifically different types of Gulls, such as Western, California, Herring, and Slaty-Backed Gulls. We observe that the top-activating images for these classes share all concepts in common which is not the case with dimension 3067. For feature 3067, as shown in Figure 2 (right) we observe that the top-activating images share common visual attributes, such as a white-colored throat and black eyes. Through human qualitative evaluation, we find that **features in the sparse latent space capture meaningful visual concepts, grouping semantically similar images together, either from the same class or across different classes, as long as they share underlying conceptual similarities.**

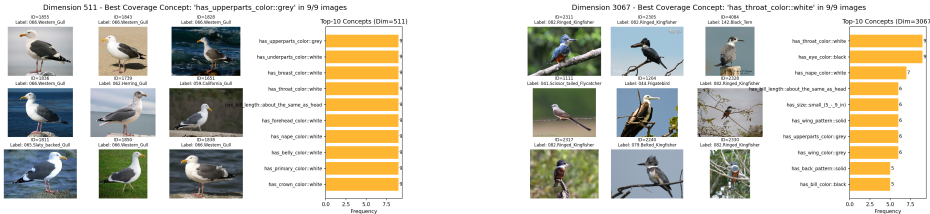


Figure 2: Concept coverage analysis of learned sparse latent features in the Sparse Autoencoder (SAE). Each subfigure illustrates the top-activating images for two different SAE dimensions, highlighting the consistency of shared visual concepts among the highest-activated examples. The analysis demonstrates how sparse features capture meaningful semantic attributes, grouping semantically similar images either within or across classes. **Left:** Top-activating images for feature 511. The images predominantly belong to different classes of Gulls (e.g., Western, California, Herring, and Slaty-Backed Gulls), yet they share consistent visual characteristics such as a gray upper part and a white underpart. This suggests that feature 511 captures a semantically meaningful concept spanning multiple related categories. **Right:** Top-activating images for feature 3067. The images share distinct visual attributes, including a white-colored throat and black eyes. However, unlike feature 511, these images belong to more diverse categories, indicating that this latent dimension captures a broader concept that generalizes across different classes.

B Sensitivity to Sparse Amplification (γ) and Steering Magnitude (λ)

We analyze how the two key hyperparameters in VS2 (i) the sparse-feature amplification γ , and (ii) the steering vector scale λ affect downstream accuracy. In the absence of contrastive supervision, these parameters govern how strongly we amplify sparse activations and how far the embedding is shifted in feature space. We sweep both values across a grid on three datasets: CIFAR-100, CUB-200, and Tiny-ImageNet using ViT-B/32 backbone.

Figure 3 shows that all tested combinations of (λ, γ) outperform the zero-shot baseline, though to varying degrees. Each dataset exhibits a diagonal band of near-optimal settings where $\lambda \cdot \gamma \in [2, 3]$ tends to yield peak accuracy. For example, CIFAR-100 peaks at $\lambda^* = 2.1$ and $\gamma^* = 1.5$. Beyond this band, increasing λ or γ causes performance to degrade likely due to over-amplification of sparse codes and embedding distortion. The consistent contour patterns across datasets suggest that VS2 is robust to moderate variation in its hyperparameters and that good settings generalize well across domains.

C Training top- k Sparse Autoencoders

We follow CLIP [18] with a ViT-B/32 and ViT-B/16 vision backbones, intercepting the output of each encoder layer for the CLS token. Specifically, we train top- k SAEs on the CLS embeddings for each chosen layer. We use $k = 64$ and $k = 256$ as the maximum active features within the latent space for ViT-B/32 and ViT-B/16 respectively, and we set a “dead feature” threshold of 100 i.e., any feature seldom activated is pruned. We also use an expansion factor of 4 relative to the input embedding dimension, resulting in 3,072 latent units. Training largely follows [31] and uses [53], with a linear learning-rate schedule and warmup from 5×10^{-4} .

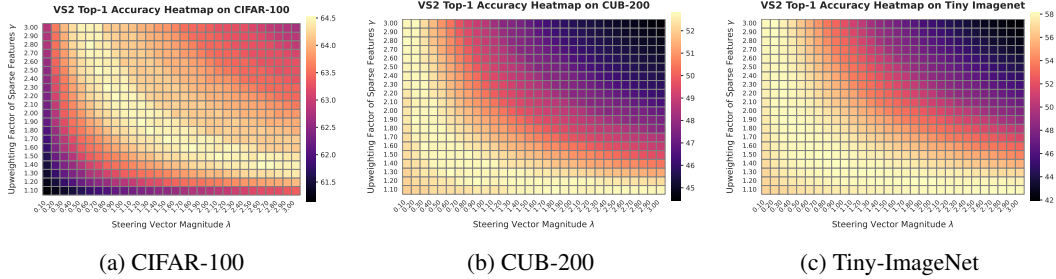


Figure 3: **Sensitivity of VS2 to sparse amplification γ and steering magnitude λ .** All three datasets show a range of near-optimal combinations (warm colours), typically when $\lambda \cdot \gamma \in [2, 3]$. Accuracy degrades if either parameter becomes too large.

Table 4: **Fraction of variance unexplained (FVU; lower is better).** Each SAE has 4 \times expansion; sparsity $k = 64$ for ViT-B/32 and $k = 256$ for ViT-B/16.

Dataset	ViT-B/32 ($k=64$)	ViT-B/16 ($k=256$)
CIFAR-100	0.2812	0.1166
CUB-200	0.2487	0.1653
Tiny-ImageNet	0.5060	0.3018

We monitor reconstruction quality with the **fraction of variance unexplained (FVU; lower is better)**, defined as

$$\text{FVU} = \frac{\|\mathbf{X} - \hat{\mathbf{X}}\|_F^2}{\|\mathbf{X} - \bar{\mathbf{X}}\|_F^2}, \quad (20)$$

where $\mathbf{X} \in \mathbb{R}^{B \times d}$ is a batch of CLS embeddings, $\hat{\mathbf{X}}$ denotes their SAE reconstructions, and $\bar{\mathbf{X}}$ is the batch mean (so the denominator equals the total variance). FVU is the complement of the coefficient of determination ($1 - R^2$); an FVU of 0 indicates perfect reconstruction, while an FVU of 1 corresponds to predicting only the mean. In Table 4, we report FVU results for ViT-B/32 with $k = 64$ and ViT-B/16 with $k = 256$ across all three datasets.

D Sensitivity in Retrieval-Augmented Generation (RAG)

When an external image corpus is available, VS2 can be extended using a Retrieval-Augmented Generation (RAG) pipeline. We use DINOv2 [50] to retrieve top- k images most similar to the input query and compute an enhanced embedding by combining the query with the retrieved set:

$$\mathbf{E} = \alpha \mathbf{q} + (1 - \alpha) \sum_{j=1}^k w_j \mathbf{r}_j,$$

where \mathbf{q} is the query embedding, \mathbf{r}_j the j -th retrieved embedding, and w_j the normalized similarity weight:

$$w_j = \frac{s_j}{\sum_{i=1}^k s_i}, \quad \text{where } s_j = \text{sim}(\mathbf{q}, \mathbf{r}_j).$$

The parameter $\alpha \in [0, 1]$ controls the trade-off between using the original query and the retrieved set.

We sweep over values of α and k to assess their impact on zero-shot classification performance. Figure 4 shows results for CIFAR-100, and Tiny-ImageNet.

Findings. CIFAR-100 and Tiny-ImageNet display a similar trend: larger α (i.e., more reliance on the query) typically degrades performance. On Tiny-ImageNet, setting $\alpha = 0$, completely ignoring the input query and relying purely on retrieved features, yields the best result. This suggests that the retrieval set carries strong distributional signal in cluttered datasets. Across all datasets, large k eventually hurts performance, confirming that RAG benefits from focused rather than broad context.

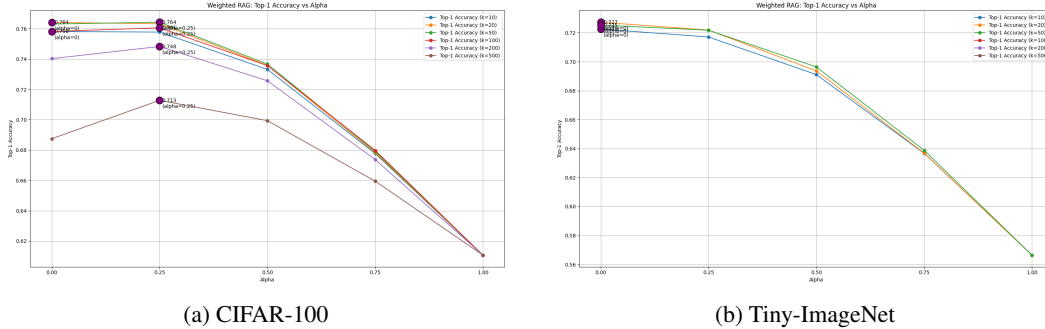


Figure 4: **RAG sensitivity to α and top- k .** Accuracy varies with the weight α on the original query and the number k of retrieved images. Larger k often introduces noise; smaller α performs better on cluttered datasets.

The trade-off parameter α and the retrieval depth k play dataset-dependent roles in RAG-enhanced pipelines. For fine-grained domains, fewer, high-confidence neighbors and a low α work best; for noisy domains, more reliance on the retrieval pool is beneficial.

E Are exemplar-derived directions really distinct?

A desirable property of class-specific steering vectors is *orthogonality*: pushing an embedding toward class A should not simultaneously raise its score for class B . Using the oracle prototypes as described in Section 4.2, we compute for every CIFAR-100 class a prototype steering vector and measure the pair-wise cosine similarity at layer 11 of the ViT-B/32 encoder. Most pairs have low similarity (mean = 0.23), yet a non-negligible tail reveals strongly overlapping directions. Table 5 lists the ten highest-overlap pairs:

Table 5: **Top-10 most overlapping prototype steering directions on CIFAR-100.** High cosine similarity indicates that the two classes share visual attributes that the SAE encodes along nearly the same latent axis.

Rank	Class 1	Class 2	Cosine \uparrow
1	beetle	cockroach	0.91
2	mouse	shrew	0.89
3	dolphin	shark	0.84
4	otter	seal	0.84
5	dolphin	whale	0.84
6	possum	raccoon	0.84
7	snake	worm	0.83
8	oak tree	willow tree	0.83
9	ray	shark	0.81
10	bowl	cup	0.80

These high-overlap pairs are *semantically plausible* confusions (e.g. beetle vs. cockroach or dolphin vs. whale), confirming that exemplar steering directions tend to align for visually or taxonomically proximate classes. In downstream applications, a simple orthogonalization step may help reduce feature overlap between sparse directions. Investigating principled ways to encourage orthogonality during SAE training is a promising direction for future work.

F Ablation Study of Expansion factor and top- k

In Table 6, we present the downstream task accuracy of CLIP ViT-B/32 using various values of expansion factor and k . Across a $4 \times$ range in width and an $8 \times$ range in sparsity, top-1 accuracy fluctuates by less than one percentage point *evidence that VS2’s performance is largely insensitive to the precise SAE capacity-sparsity trade-off*. Additionally, in Table 7, we present the average cosine

similarities of different steering vectors coming from various configurations of SAEs in terms of expansion factor and top- k .

Table 6: **VS2 accuracy as a function of SAE width (expansion factor) and sparsity (top- k).** Numbers are top-1 / top-5 (%). The best result is boldfaced; every other configuration is within of the optimum, highlighting the method’s robustness to architectural choices.

SAE configuration	Top-1 \uparrow	Top-5 \uparrow
$4 \times, k=128$	64.61	87.95
$8 \times, k=128$	64.56	87.76
$4 \times, k=64$	64.54	87.79
$16 \times, k=64$	64.54	87.78
$8 \times, k=64$	64.52	87.96
$10 \times, k=128$	64.43	87.81
$16 \times, k=512$	64.42	87.71
$8 \times, k=512$	64.40	87.91
$4 \times, k=256$	64.34	87.62
$8 \times, k=256$	64.29	87.80
$16 \times, k=256$	64.28	87.75
$4 \times, k=512$	64.12	87.87
$16 \times, k=128$	64.10	87.79

G Visual Sparse Steering Pseudocode

For reproducibility purposes, in Algorithm 1, we provide the pseudocode for the baselines and VS2 used in the analysis of 4.1.1.

Algorithm 1 SAE_STEERING – SAE-based CLS token modification

```

1: function SAE_STEERING( $\mathbf{h}$ , SAE,  $k$ ,  $\gamma$ ,  $\lambda_{\Delta z}$ , mode)  $\triangleright$   $\mathbf{h}$ : CLS token; SAE: sparse autoencoder;
    $k$ : sparsity level
2:    $\mathbf{a}, \mathbf{idx} \leftarrow$  SAE.select_topk(SAE.pre_acts( $\mathbf{h}$ ),  $k$ )
3:    $\mathbf{z}_{\text{base}} \leftarrow$  SAE.decode( $\mathbf{a}, \mathbf{idx}$ )
4:    $\mathbf{z}_{\text{boost}} \leftarrow$  SAE.decode( $\gamma \cdot \mathbf{a}, \mathbf{idx}$ )
5:   if mode = "reconstruction" then
6:     return  $\mathbf{z}_{\text{base}}$   $\triangleright$  Variant: CLIPRECF
7:   else if mode = "amplified" then
8:     return  $\mathbf{z}_{\text{boost}}$   $\triangleright$  Variant: CLIPRECF+\gamma
9:   else if mode = "steering" then
10:    return  $\mathbf{h} + \lambda_{\Delta z} \cdot (\mathbf{z}_{\text{boost}} - \mathbf{z}_{\text{base}})$   $\triangleright$  VS2
11:   end if
12: end function

```

H Comparison with other Baseline Methods

We compare VS2 against SpLiCE [16], using the official implementation provided by the authors. For all three datasets, we report performance using SpLiCE with an external vocabulary of 10,000 LAION-based concepts and an ℓ_1 regularization weight of 0.25, following their best reported configuration. Despite relying on no external vocabulary, VS2 consistently outperforms SpLiCE across all benchmarks highlighting the strength of sparse concept steering even in the absence of external lexical resources.

Table 8: Zero-shot top-1 accuracy (%) on **CIFAR-100**.

Method	ViT-B/32	ViT-B/16
CLIP _{ZS}	61.07 (0)	63.96 (0)
SAE _{REC} ^A	58.01 (-3.06)	64.05 (+0.09)
SAE _{REC} ^F	58.22 (-2.85)	63.42 (-0.54)
SAE _{REC} ^{F+γ}	62.69 (+1.62)	66.81 (+2.85)
SpLiCE [16]	55.57 (-5.50)	58.29 (-5.67)
VS2 (ours)	64.52 (+3.45)	68.08* (+4.12)

I Effect of Top- N Retrieved Neighbors

To assess the influence of retrieval size on performance, we conduct an ablation over the number of retrieved neighbors N used for latent aggregation. We use a fixed ViT-B/16 (Patch-16) backbone and vary $N \in \{10, 25, 50, 100\}$ across three datasets: CIFAR-100, CUB-200, and Tiny-ImageNet. As shown in Figure 5, both top-1 and top-5 classification accuracy steadily increase with N on CIFAR-100 and Tiny-ImageNet, with diminishing returns beyond $N = 50$. In contrast, performance on CUB-200 remains largely flat or slightly degrades, suggesting that retrieving more neighbors in fine-grained datasets can introduce noise due to overly similar but semantically irrelevant examples. These results indicate that the utility of neighbor-based aggregation is dataset-dependent: general object recognition tasks benefit from larger N , while fine-grained classification may require more careful control of retrieval scope.

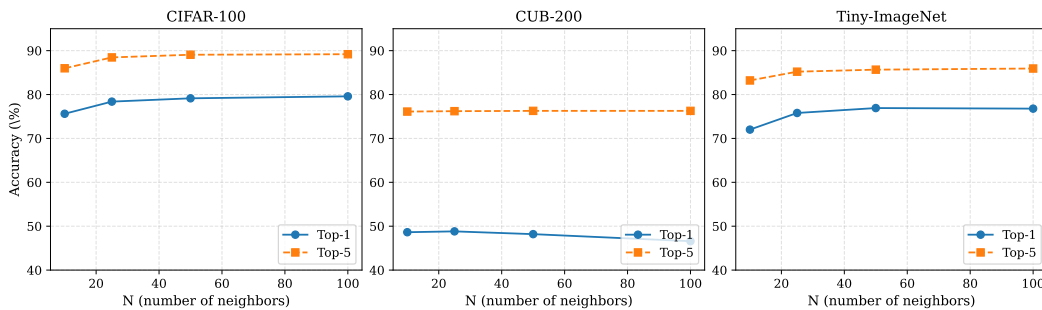


Figure 5: Top-1 and Top-5 accuracy as a function of number of retrieved neighbors N , using ViT-B/16 (Patch-16) across datasets. Larger N improves general classification but may degrade performance in fine-grained settings.

J Per-class Performance Analysis on CIFAR-100

In Table 9, we present results for the classes most affected by steering CLIP ViT-B/32 with VS2 and VS2⁺⁺. We highlight both positive and negative shifts in accuracy to identify the most impacted categories. Unlike the average performance reported in the main experiments, this analysis shows that the top-10 class-level gains are generally larger in magnitude than the corresponding losses. Although the accuracy drops for misclassified categories are smaller in magnitude, they are non-negligible. As future work, it would be valuable to explore when steering should be applied or withheld to further maximize overall performance gains.

Table 7: Cosine similarity (\uparrow) between steering vectors learned by different SAE capacities. Rows/columns are ordered by expansion factor and sparsity ($e \times$ expansion, k active).

SAE cfg.	16x/64	16x/512	16x/128	16x/256	8x/128	8x/512	8x/256	4x/256	4x/512	4x/128	10x/128	4x/64	8x/64
16x/64	1.000	0.497	0.577	0.705	0.726	0.635	0.680	0.640	0.591	0.681	0.536	0.701	0.716
16x/512	0.497	1.000	0.161	0.399	0.358	0.817	0.634	0.618	0.611	0.584	0.136	0.316	0.282
16x/128	0.577	0.161	1.000	0.900	0.865	0.273	0.298	0.277	0.265	0.303	0.952	0.887	0.678
16x/256	0.705	0.399	0.900	1.000	0.956	0.527	0.572	0.495	0.410	0.542	0.920	0.936	0.744
8x/128	0.726	0.358	0.865	0.956	1.000	0.543	0.650	0.575	0.483	0.634	0.896	0.959	0.829
8x/512	0.635	0.817	0.273	0.527	0.543	1.000	0.861	0.811	0.771	0.796	0.243	0.483	0.506
8x/256	0.680	0.634	0.298	0.572	0.650	0.861	1.000	0.889	0.771	0.912	0.289	0.557	0.624
4x/256	0.640	0.618	0.277	0.495	0.575	0.811	0.889	1.000	0.873	0.941	0.240	0.532	0.600
4x/512	0.591	0.611	0.265	0.410	0.483	0.771	0.771	0.873	1.000	0.821	0.191	0.461	0.549
4x/128	0.681	0.584	0.303	0.542	0.634	0.796	0.912	0.941	0.821	1.000	0.284	0.594	0.655
10x/128	0.536	0.136	0.952	0.920	0.896	0.243	0.289	0.240	0.191	0.284	1.000	0.910	0.678
4x/64	0.701	0.316	0.887	0.936	0.959	0.483	0.557	0.532	0.461	0.594	0.910	1.000	0.814
8x/64	0.716	0.282	0.678	0.744	0.829	0.506	0.624	0.600	0.549	0.655	0.678	0.814	1.000

Table 9: **Top-10 class gains and losses on CIFAR-100.** Green = absolute gain; Red = absolute loss relative to ZS baseline.

(a) VS2 – Top-10 Gains			(b) VS2 – Top-10 Losses		
Class	ZS	VS2 $\uparrow(\Delta)$	Class	ZS	VS2 (Δ)
tractor	0.55	0.80 $\uparrow(+0.25)$	aquarium_fish	0.82	0.61 (-0.21)
forest	0.35	0.58 $\uparrow(+0.23)$	beetle	0.64	0.49 (-0.15)
man	0.53	0.74 $\uparrow(+0.21)$	sweet_pepper	0.70	0.58 (-0.12)
bus	0.51	0.68 $\uparrow(+0.17)$	tulip	0.78	0.71 (-0.07)
snake	0.61	0.76 $\uparrow(+0.15)$	maple_tree	0.57	0.50 (-0.07)
woman	0.57	0.71 $\uparrow(+0.14)$	flatfish	0.55	0.49 (-0.06)
trout	0.18	0.32 $\uparrow(+0.14)$	willow_tree	0.46	0.41 (-0.05)
cockroach	0.49	0.62 $\uparrow(+0.13)$	lamp	0.75	0.70 (-0.05)
bridge	0.72	0.83 $\uparrow(+0.11)$	lawn_mower	1.00	0.96 (-0.04)
rose	0.58	0.68 $\uparrow(+0.10)$	kangaroo	0.72	0.68 (-0.04)
(c) VS2++ – Top-10 Gains			(d) VS2++ – Top-10 Losses		
Class	ZS	VS2++ $\uparrow(\Delta)$	Class	ZS	VS2++ (Δ)
spider	0.48	0.91 $\uparrow(+0.43)$	girl	0.72	0.65 (-0.07)
caterpillar	0.27	0.68 $\uparrow(+0.41)$	maple_tree	0.57	0.51 (-0.06)
possum	0.24	0.65 $\uparrow(+0.41)$	porcupine	0.18	0.13 (-0.05)
tractor	0.55	0.96 $\uparrow(+0.41)$	ray	0.06	0.02 (-0.04)
tiger	0.45	0.84 $\uparrow(+0.39)$	mouse	0.18	0.15 (-0.03)
raccoon	0.44	0.83 $\uparrow(+0.39)$	lawn_mower	1	0.98 (-0.02)
lizard	0.36	0.74 $\uparrow(+0.38)$			
wolf	0.54	0.90 $\uparrow(+0.36)$			
shrew	0.44	0.79 $\uparrow(+0.35)$			
bear	0.51	0.85 $\uparrow(+0.34)$			